NMR Structure of the Cathelicidin-Derived Human Antimicrobial Peptide LL-37 in Dodecylphosphocholine Micelles†

Fernando Porcelli,‡,§ Raffaello Verardi,‡ Lei Shi,‡ Katherine A. Henzler-Wildman,|| Ayyalusamy Ramamoorthy,*,|| and Gianluigi Veglia*,‡

Department of Biochemistry, Molecular Biology and Biophysics and Department of Chemistry, University of Minnesota, Minneapolis, Minnesota 55455, Department of Environmental Sciences (Di.S.A.), University of Tuscia, Viterbo, Italy, and Department of Chemistry and Biophysics, University of Michigan, Ann Arbor, Michigan 48109-1055

Received October 10, 2007; Revised Manuscript Received March 18, 2008

ABSTRACT: LL-37 is the only cathelicidin-derived polypeptide found in humans. Its eclectic function makes this peptide one of the most intriguing chemical defense agents, with crucial roles in moderating inflammation, promoting wound healing, and boosting the human immune system. LL-37 kills both prokaryotic and eukaryotic cells through physical interaction with cell membranes. In order to study its active conformation in membranes, we have reconstituted LL-37 into dodecylphosphocholine (DPC) micelles and determined its three-dimensional structure. We found that, under our experimental conditions, this peptide adopts a helix−break−helix conformation. Both the N- and C-termini are unstructured and solvent exposed. The N-terminal helical domain is more dynamic, while the C-terminal helix is more solvent protected and structured (high density of NOEs, slow H/D exchange). When it interacts with DPC, LL-37 is adsorbed on the surface of the micelle with the hydrophilic face exposed to the water phase and the hydrophobic face buried in the micelle hydrocarbon region. The break between the helices is positioned at K12 and is probably stabilized by a hydrophobic cluster formed by I13, F17, and I20 in addition to a salt bridge between K12 and E16. These results support the proposed *nonpore carpet-like* mechanism of action, in agreement with the solid-state NMR studies, and pave the way for understanding the function of the mature LL-37 at the atomic level.

The increasing bacterial resistance to conventional antibiotic compounds is an urgent problem to be addressed. Natural antimicrobial peptides are one of the first evolved chemical defense mechanisms of eukaryotic cells against bacteria, protozoa, fungi, and viruses (*1, 2*). The broad spectrum antibacterial activity, high selectivity, and the disruption of bacterial cell membranes exhibited by hundreds of antimicrobial peptides suggest that these molecules are potentially useful as antibiotics; therefore, it is important to investigate their structure and function at high resolution in order to increase their potency and selectivity. Interestingly, there is no amino acid sequence homology among these peptides. On the other hand, their ability to interact with lipid membranes depends highly on their secondary and tertiary structures. Therefore, high-resolution structures of these peptides in a suitable membrane environment are essential to understand their mechanism of action. While X-ray crystallography can be used to solve the structures of these peptides when they can be prepared as a single crystal, it is difficult to obtain a single crystal of these short AMPs in a membrane environment. Therefore, solid-state NMR spectroscopy in lipid bilayers and solution NMR spectroscopy in micelles are the most suitable techniques to solve the structures of AMPs at high resolution. In this study, we have solved the high-resolution structure of the *only* cathelicidin-derived human antimicrobial peptide, LL-37, using solution NMR spectroscopy in detergent micelles.

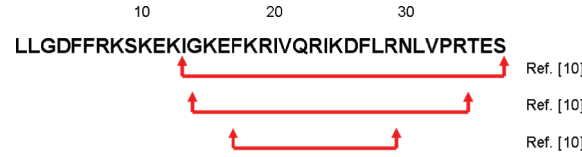

FIGURE 1: Primary amino acid sequence of LL-37. The regions defined by the arrows indicate the active polypeptides identified by different research groups.

Cathelicidins are a well-known family of structurally diverse antimicrobial peptides that are linked at the carboxyl terminus to a 15−18 kDa highly conserved cathelin-like domain (cathepsin L inhibitor) (*3*). LL-37 is expressed as a *pro*-peptide (hCAP18) within neutrophils (and testes) and then cleaved into a 4.5 kDa mature peptide. The primary sequence of LL-37 is reported in Figure 1. LL-37 has cytotoxic activity against both Gram-positive and Gram-negative bacteria, demonstrating synergistic effects with lactoferrin and human defensin HNP-1. Electron micrographs of bacteria exposed to LL-37 show typical cell death profiles,

† NMR instrumentation at the University of Minnesota High Field NMR Center was funded by the National Science Foundation (BIR-961477) and the University of Minnesota Medical School. This research was supported by research funds from the NIH (AI054515 to A.R. and GM 64742 and HL0800081 to G.V.).

* To whom correspondence should be addressed. G.V.: tel, (612) 625-0758; fax, (612) 625-2163; e-mail, veglia@chem.umn.edu. A.R.: tel, (734) 647-6572; e-mail, ramamoor@umich.edu.

‡ University of Minnesota.

§ University of Tuscia.

|| University of Michigan.

10.1021/bi702036s CCC: $40.75
Published on Web 04/26/2008

with membrane blebbing and lysis at the peptide minimal inhibitory concentration (MIC). However, for some eukaryotic cell lines LL-37 displays a cytotoxicity at MIC greater than 5 times that of the bacterial cells.

LL-37 has also been detected in human wounds and blister fluids, and more recently the gene coding for LL-37 was found to be induced in human keratinocytes during inflammation (*4*−*6*). LL-37 may play a critical role in cystic fibrosis remediation, where inactivation of human β-defensin-1 compromises the innate immunity of the lung, leading to frequent bacterial infections (*7*). Under these pathologic conditions, LL-37 is able to restore normal levels of *Pseudomonas aeruginosa* and *Staphylococcus aureus* killing (*8, 9*). More recently Söderlund and co-workers evaluated the ability of LL-37 to inhibit HIV-1 infection *in vitro* (*10*). These researchers found that LL-37 inhibits HIV-1 replication in primary CD4(+) T cells, showing that this peptide may contribute to the local protection against HIV-1 infection. All of these biological data suggest that LL-37 function may extend beyond its antimicrobial activity, including wound healing, chemotactic attraction of leukocytes, and modulation of the inflammatory response (*11*). More details on various biological functions and physicochemical properties of this intriguing molecule are well covered in a recently published review article by Durr et al. (*11*).

Unlike defensins, LL-37 retains a broad-spectrum bactericidal activity with a high rate of microbial killing at both physiological and elevated salt concentrations. In addition, LL-37 is devoid of disulfide bridges and forms stable oligomers protected from proteolytic degradation. Unlike other antimicrobial α-helical amphipathic peptides, LL-37 binds and permeates both zwitterionic and negatively charged membranes and is resistant to proteolysis when bound to phospholipids in either monomeric or oligomeric states. These features make LL-37 an excellent lead for drug design. Using a minimalist approach, several groups studied truncated versions of LL-37 with the goal of improving its antimicrobial action and identifying a small template to design new therapeutic approaches (*11*). Originally, the most active region was limited to about 20 residues, while more recent studies using a TOCSY-trim approach permitted further reduction of the active polypeptide down to 13 residues without jeopardizing the peptide activity (*12*) (Figure 1).

Given its small size, LL-37 has been the target of several structural and spectroscopic investigations. In particular, circular dichroism (CD) studies helped to characterize LL-37 secondary structure as well as its oligomerization state. It was found that LL-37 assumes a random coil conformation in aqueous solutions and adopts a helical structure in both organic solvents and membrane-mimicking environments such as detergent micelles. Using CD in conjunction with activity assays, Johansonn et al. found that both the helical conformation and oligomerization of LL-37 are important for cytotoxic action of the peptide (*13*). In addition, recent solid-state NMR studies provided an initial characterization of the conformation, dynamics, orientation, and oligomeric nature of LL-37 in membranes (*14*). The mechanism of membrane disruption by LL-37 in model membrane bilayers with various lipid compositions was also reported (*15*). The helical propensity of LL-37 has been reiterated by a few recent papers, describing fully functional fragments of this peptide solubilized in SDS as well as D8PG micelles (*12*). Taken with structural predictions, these studies identified the helical nature of LL-37 and the possibility of breaks into the secondary structure. To date, however, the lack of resolution in the NMR spectra and the inability to crystallize this peptide prevented the determination of the complete high-resolution structure.

Here, we present the high-resolution structure and the topology of LL-37 in complex with dodecylphosphocholine (DPC) micelles as a membrane-mimicking environment. Taken with the recent solid-state NMR results, these new data offer a more realistic picture of how this peptide interacts with membranes.

MATERIALS AND METHODS

Materials. All of the reagents for peptide synthesis and cleavage were purchased from Applied Biosystems (Foster City, CA) and Aldrich (Milwaukee, WI), respectively. Fmoc-protected amino acids were from Advanced ChemTech (Louisville, KY), and isotopically labeled Fmoc-amino acids and perdeuterated DPC were from Cambridge Isotope Laboratories (Cambridge, MA). Chloroform and methanol were from Aldrich (Milwaukee, WI), and all other reagents were from Fisher (Pittsburgh, PA).

Peptide Synthesis. LL-37 was synthesized on an ABI-431A (Applied Biosystems, Foster City, CA) peptide synthesizer using FastMoc chemistry with double coupling and double deprotection. The peptide was cleaved from the Ser(*t*-Bu)-Wang resin (Peptides International, Louisville, KY) to produce a free carboxylate at the C-terminus. Removal of protecting groups was accomplished using trifluoroacetic acid (TFA) and scavengers. The peptide was purified using reversed-phase high-pressure liquid chromatography on a C8 column (Vydac). The residual TFA was washed out using a solution with 1% acetic acid. It was essential to remove the residual TFA from the sample as its presence altered the property of lipid bilayers as determined from ^{31}P solid-state NMR experiments. The molecular mass and the purity of the samples were characterized by mass spectrometry and analytical HPLC (molecular mass of ~4.5 kDa with >96% purity).

NMR Sample Preparation. Before preparing NMR samples, LL-37 was dissolved in a chloroform−methanol−water (4:4:1 v/v) solution. The solvent mixture was evaporated under nitrogen flux, and the peptide was lyophilized. The NMR samples were prepared by dissolving the lyophilized peptides in an aqueous solution (10% ^2H_2O, 90% H_2O) containing 300 mM perdeuterated DPC (Cambridge Isotope Laboratories) and 20 mM phosphate buffer at pH ~6 at a final concentration of 1.5 mM. To detect the NOEs between LL-37 and detergent molecules, the NMR sample was doped with 10% protonated DPC.

To determine the location of LL-37 with respect to the micelle, the sample was doped with gadopentetate dimeglumine (Gd^{3+} for simplicity).

Dynamic Light Scattering. The size of the micelle/LL37 complex was evaluated by dynamic light scattering (DLS). All of the measurements were carried out at 298 K using a DynaPro (Protein Solutions) Titan (Wyatt Technology Corp.) with a vertical polarized light of 488 nm wavelength.

Samples both in the absence of peptide and in the presence of different DPC/peptide molar ratios were prepared in 20 mM phosphate buffer at pH 6.0 and centrifuged for 10 min at 5000 rpm prior to each measurement.

NMR Spectroscopy. All of the NMR experiments were performed at 300 K on a Varian Inova 600 MHz spectrometer. The 2D [^{1}H,^{1}H] total correlation spectroscopy (TOCSY) (*16*) (50 and 65 ms mixing time) and 2D [^{1}H,^{1}H] NOESY (*17*) (50−300 ms mixing time) experiments were run in the phase-sensitive mode using time-proportional phase incrementation (TPPI) for quadrature detection in the indirect dimension. All of the pulse sequences utilized a WATERGATE pulse scheme (*18*) for solvent suppression. The experiments were acquired with 256 and 1024 complex data points in the ω_1 and ω_2 dimensions, respectively. A DIPSI-2 pulse sequence (*19*) was used for isotropic mixing in the 2D TOCSY experiments. The spectral widths were 8000 Hz in both the ω_1 and ω_2 dimensions. To determine the location of LL-37 with respect to the micelle, three 2D [^{1}H,^{1}H] NOESY experiments (70 ms mixing time) were collected: the first in the absence of Gd^{3+}, the second in the presence of 1:2 peptide:Gd^{3+} molar ratio, and a third NOESY in the presence of 1:4 peptide:Gd^{3+} molar ratio. The intensity retentions of the peptide fingerprint were reported. Proton chemical shifts were referenced to internal 3-(trimethylsilyl)propionic acid. The NMR data were processed and analyzed using NMRPipe (*20*) and SPARKY (*21*) software packages. The 2D data from all of the experiments were zero-filled to 4096 points in ω_2 and to 1024 points in ω_1 and then processed with a sine-bell squared window function shifted between 60° and 90° as appropriate before Fourier transformation. A polynomial of sixth order was used for baseline correction in both frequency dimensions. Spectra were assigned using a standard assignment approach described by Wuthrich (*22*). A table with all of the assigned resonances is provided in the Supporting Information.

Structure Calculations. NOE cross-peaks from the 250 and 300 ms mixing time NOESY experiments were integrated and used for the structure calculations. The NOE volumes were calibrated using the average NOE volume from resolved aromatic vicinal protons of F27 and classified as strong, medium, and weak, corresponding to distance restraints of 1.8−2.9, 1.8−4.5, and 1.8−5.0 Å, respectively. Solvent accessibility of the amide backbone signals was determined by proton/deuterium exchange studies. Samples were prepared by dissolving the lyophilized protein sample in fully deuterated DPC into ^2H_2O, and solvent accessibility was monitored by following the disappearance of the $H_\alpha-H_N$ cross-peaks by 2D NOESY spectra. After a period of 24 h, most of the resonances of the N-terminal portion of the polypeptide had disappeared, while the most solvent-protected residues (residues 9 and 29) were still detectable after several days.

Final structures of LL-37 were calculated starting from an extended conformation using the simulated annealing (SA) protocol available in XPLOR-NIH (*23*). A total of 100 conformers were generated using random seed at an initial temperature of 5000 K with 6000 high-temperature steps, 3000 cooling steps, and a step size of 5 fs. The final target function included a total of 348 NOEs (130 intraresidue and 218 interresidue distances). In addition, 17 hydrogen bond constraints were implemented using NH−CO (i, i + 4) distance restraints from I13 through R29. The final stage of refinement of the structural ensemble was carried out starting at an initial temperature of 500 K and using 30000 cooling steps with a 1 fs step size. The 70 refined structures had no NOE violations >0.5 Å, no bond violations >0.05 Å, and no bond angle violations >4°. The 40 lowest energy conformers were then selected for further analysis. The analysis of Ramachandran angles for the 48 lowest energy structures was carried out using PROCHECK-NMR (*24*). For the final conformers, the occurrence of the ϕ and ψ angles for all of the residues in the Ramachandran plots was 83.6% in the most favored, 11.1% in the allowed, 1.6% in the generously allowed, and 3.7% in disallowed regions. The residues located in the N- and C-termini, which had fewer structural restraints, account for those residues found in the disallowed regions of the Ramachandran plots.

The orientation of LL-37 with respect to the micelle was determined using a *pseudomicelle potential* (*25*). In short, we first estimated the size of the DPC micelle from DLS data (see above). We calculated an average of ~60 monomers per micelle in the presence of the peptide. According to Tieleman and co-workers (http://www.ucalgary.ca/~tieleman/download.html), this corresponds to a micelle radius of ~20 Å. To model the distances obtained from Gd^{3+} paramagnetic quenching experiments and the detergent−peptide NOEs, we assumed a spherical size of the micelle with a pseudoatom positioned in the center of micelle. Upper and lower bounds of 4 Å were defined using the classical convention for paramagnetic relaxation enhancement (PRE) data established by Battiste and Wagner (*26*). For residues located outside the micelle (see Gd^{3+} data) we imposed harmonic distance restraints for their amide protons greater than 16 Å from the center of the micelle. For residues located inside the micelle, we imposed harmonic distance restraints less than 16 Å from the center of the micelle. We will refer to these distances as *pseudomicelle* restraints. Indeed, we used a conservative approach, considering outside the micelles only those residues with ~100% of intensity retention and inside the micelle those residues with intensity retention less than 50%.

RESULTS

Previous NMR investigations focused on functional fragments of LL-37 solubilized in SDS or D8PG micelles. However, the 2D spectra of full-length unlabeled, synthetic LL-37 under these experimental conditions were poorly resolved and did not allow for full structure determination (*12*). For our structural analysis, the full-length synthetic LL-37 was reconstituted in DPC micelles. We chose DPC as a detergent because of the high affinity of LL-37 for zwitterionic membranes containing phosphatidylcholine (*11, 14*). Peptide concentration, pH, and ionic strength as well as peptide/detergent ratios were carefully scanned to obtain a high-resolution peptide fingerprint. The size of the micelle/peptide complex was estimated by DLS. In the absence of peptide, we found that the hydrodynamic radius (HR) for DPC micelles in the absence of LL37 is 24 ± 2 Å with a molecular mass of ~26 kDa. In the presence of peptide, we observed only a slight increase of HR (~26 ± 2 Å). However, the estimated molecular mass was 30 kDa, which fits well with the increase in molecular mass upon addition of LL-37.

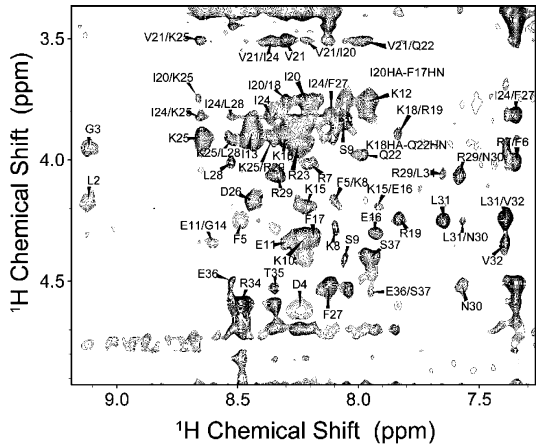

FIGURE 2: Fingerprint region of LL-37 extracted from a 2D [^{1}H−^{1}H] NOESY experiment at 300 ms mixing time. The sample consisted of 1 mM LL-37 reconstituted into phosphate buffer containing 300 mM DPC at pH 6.0.

To assign the backbone and side chain resonances, a combination of 2D [^{1}H,^{1}H]-TOCSY and NOESY spectra at different mixing times was used. As an example, the fingerprint region of the NOESY spectrum at 300 ms of mixing time is shown in Figure 2. The complete resonance assignment is given in Table 1 in the Supporting Information. With the exception of the $H_\alpha-H_N$ correlations for L1 and P33 residues, which are absent in the spectra, all of the resonances in the fingerprint region were assigned. However, due to the inefficient relay of the magnetization in the TOCSY experiments only a few residues displayed complete spin systems, while the $H_\alpha-H_N$ cross-peaks were detected for most of the residues. The latter allowed us to "walk" through the polypeptide backbone and perform most of the sequential assignment (*22*). From the analysis of the 2D NOESY spectra, we identified and assigned a total of 348 NOEs (130 intraresidue and 218 interresidue). Figure 3 shows a summary of the backbone NOEs for the secondary structure assignment with a histogram indicating the number of NOEs per residue. We detected several $d_{NN}(i, i+1)$ and $d_{\alpha N}(i, i+1)$, as well as $d_{NN}(i, i+2)$, throughout the entire peptide backbone. Also, several $d_{\alpha N}(i, i+3)$ and $d_{\alpha N}(i, i+4)$ NOE correlations diagnostic of α-helical conformation were detected from residues G2 through P33. While the highest density of NOE correlations was located between K15 and N30, there were a significant number of NOEs in the N-terminal portion of the peptide. In particular, three $d_{\alpha N}(i, i+4)$ correlations between D4 and K8, F6 and K10, and K10 and G14 suggest that the N-terminal region adopts an α-helical conformation. However, this is a weaker, more dynamic helix, based on the values of the Hα chemical shift index reported at the bottom of Figure 3 and the H/D exchange experiments. In fact, after 24 h from the sample preparation only the resonances from I13 through R29 remained solvent protected, showing $H_\alpha-H_N$ correlations in the 70 ms NOESY experiments. The C-terminal residues from 30 through 37 are unstructured and more dynamic as demonstrated by the H/D exchange experiments and the lack of long-range backbone NOEs.

Like pardaxin (*27*), magainin 2 (*28, 29*), and other peptides and proteins reconstituted in detergent micelles (*30, 31*), the quality of the spectra allowed us to assign most of the resonances but not to measure the *J* coupling constants. All

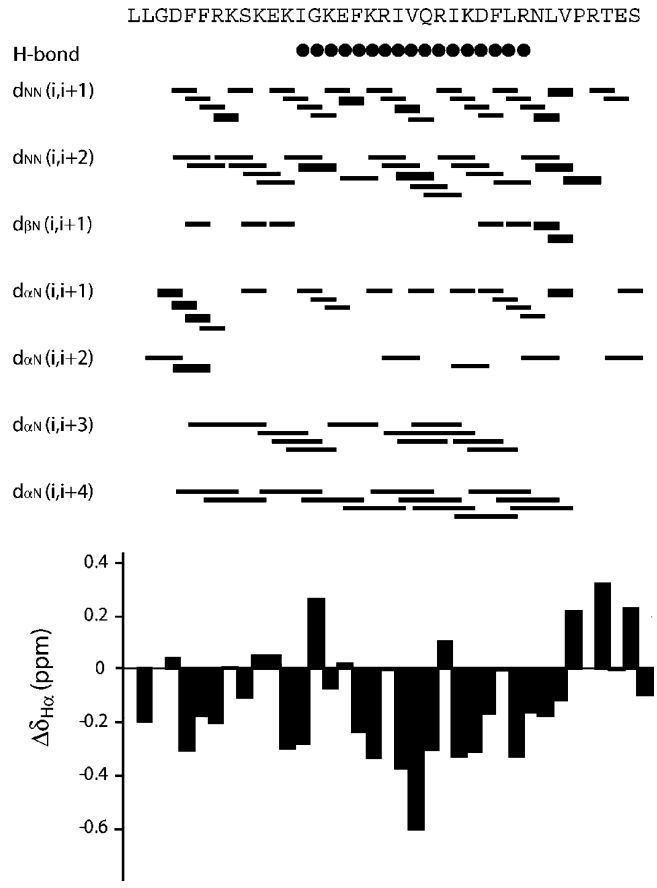

FIGURE 3: Summary of the backbone NOESY cross-peaks, Hα CSI, and H/D exchange experiments.

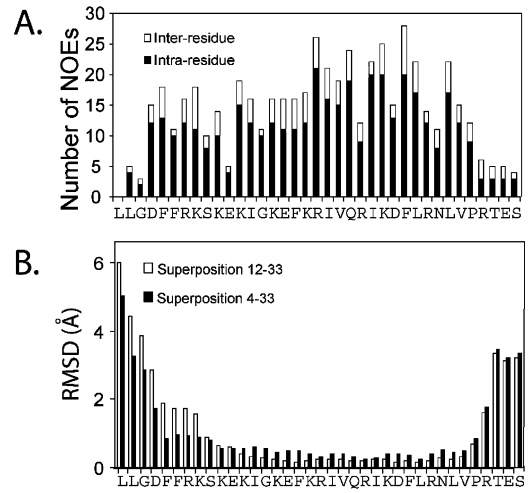

FIGURE 4: (A) Histogram of NOEs versus residues for LL-37. (B) Histogram of the backbone RMSD versus residues for the final 40 LL-37 conformers. The superpositions of the conformers from residue 4 to residue 33 and from residue 12 to residue 33 are reported.

of the NOEs and the H/D exchange data were converted into distances and modeled using the classical simulated annealing protocol built into XPLOR-NIH (*23*). Of the 70 structures calculated, 40 were selected for the final analysis. The overlays of backbone and side chain heavy atoms for the final selected conformers are reported in Figure 4. As reported in Figure 4C, the most structured region (RMSD < 1 Å) spans from residue 4 to residue 33. The superposition of the heavy backbone atoms from residue 4 to residue 33 gives an RMSD of 0.9 ± 0.2 Å, while the superposition of

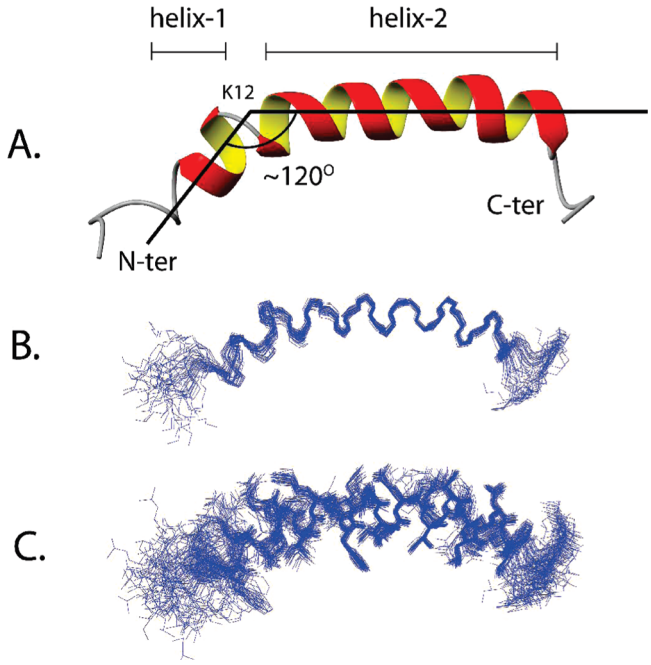

FIGURE 5: (A) Representative structure of LL-37 showing the angle between the two helical domains and the break point centered at K12. (B) Ensemble of conformers for LL-37 showing the convergence of the conformers for backbone atoms. (C) Heavy atom representation of the final calculated ensemble of conformers showing the convergence of the side chains. The structures were fit onto the relaxed average conformation.

all of the heavy atoms gives an RMSD of 1.7 ± 0.4 Å. The highest structural precision is attained if the RMSD is calculated by overlaying the backbone atoms of residues 12−33 (RMSD of 0.4 ± 0.1 Å for the backbone and 1.0 ± 0.2 Å for all of the heavy atoms). Taken with the H/D exchange measurements, these calculations support the existence of a helix−break−helix conformation of LL-37, with a more dynamic N-terminal helix, a break at K12, and a more stable conformation from residue 13 to residue 33. The hydrophobic residues reside in the concave face of the peptide, perhaps contacting the interior of the lipid bilayer. The absence of a side chain at G14 facilitates the physical contacts between I13 and F17 that form a tight cluster with I20 located in the hydrophobic face of the peptide (Figure 6). The kink induced by this hydrophobic cluster may be further stabilized by the presence of a salt bridge between K12 and E16 located on the hydrophilic face of the peptide. The presence of the salt bridge can be inferred by the close proximity of the side chains of these residues in most of the structures analyzed (Figure 6). In addition to the $d_{\alpha N}(i, i + 4)$ interactions, some of the structures of the final conformational ensemble show that the side chains of K8 and E11 are also close in space, forming a salt bridge. Both $d_{\alpha N}(i, i + 3)$ and $d_{\alpha N}(i, i + 4)$ glutamate−lysine interactions have been reported to stabilize α-helices through ion pairing, with an energy contribution of ~1 kcal/mol for solvent-exposed salt bridges (*32*). Given the occurrence of lysines in antimicrobial peptides (*33*−*38*), these types of interactions might play an important role in helix formation for amphipathic peptides upon interaction with membranes.

The topology of LL-37 in detergent micelles was obtained using a Gd^{3+} paramagnetic mapping and by direct detection of NOEs between the peptide and the detergent micelles. Figure 7A shows a plot of the intensity retention for the Hα

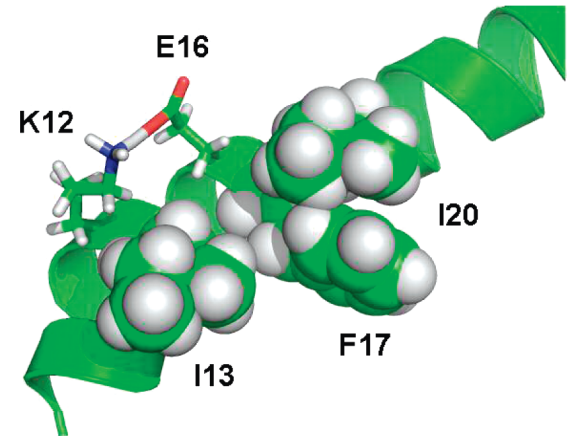

FIGURE 6: Kinked region of LL-37. The proximity of K12 and E16 side chains in most of the conformers generated using the simulated annealing procedure suggests the presence of a salt bridge between these residues. Also, the hydrophobic cluster formed by I13, F17, and I20 stabilizes the kink between the two helices.

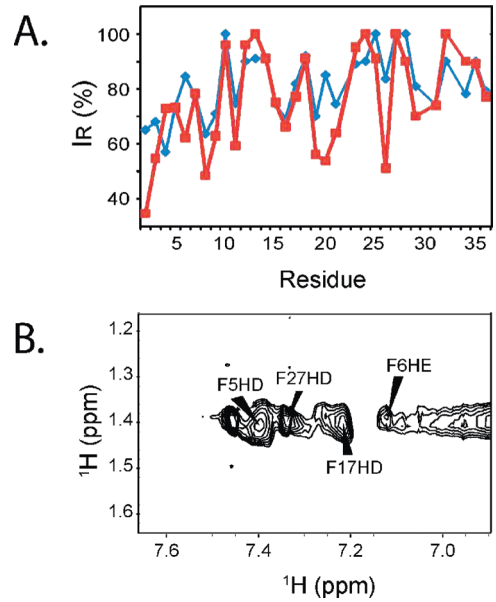

FIGURE 7: (A) Intensity retention (I_R) plots for Hα of LL-37 in the presence of 1:2 (blue trace) and 1:4 (red trace) peptide to Gd^{3+} ratios. (B) Selected region of the NOESY spectrum showing the NOEs between the aromatic residues and the methylene detergent resonances.

protons of LL-37 in the presence of Gd^{3+}. The oscillatory behavior of the intensities in the presence of the paramagnetic agent further supports the helical conformation of the peptide in interaction with the DPC micelle. In addition, to orient the hydrophobic phase of the peptide, we doped the NMR sample with 10% protonated DPC. A careful analysis of NOESY spectra reveals the presence of cross-peaks between the DPC resonances at ~1.4 ppm and the well-resolved resonances of δ protons of F5, ϵ protons of F6, and δ protons of F17 and F27 (Figure 7B). Both the paramagnetic quenching experiments and the NOEs were modeled using a *pseudomicelle* potential (see Materials and Methods). Figure 8 shows the orientation of LL-37 with respect to the micelle. As predicted from the analysis of the peptide's amphipathic nature and the secondary structure, the concave face containing the hydrophobic residues points toward the micellar interior, whereas the hydrophilic residues are oriented toward the bulk solvent.

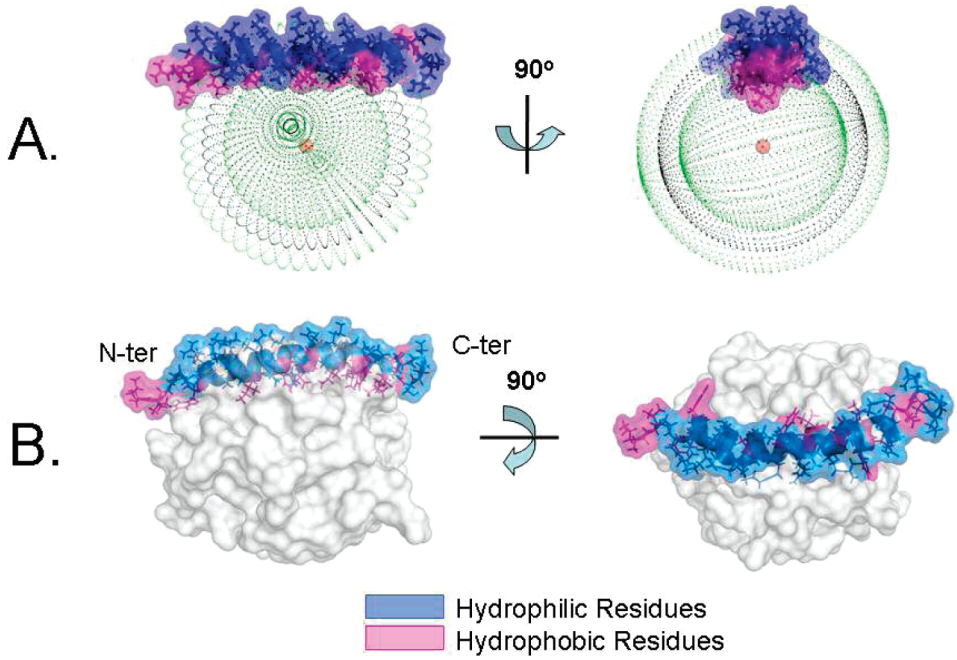

FIGURE 8: Molecular model of LL-37 embedded into a DPC micelle. (A) LL-37 orientation obtained from the *pseudomicelle* restraints. The black sphere represents the target distance (20 Å); the outer and inner spheres represent the lower and upper bounds (±4 Å). (B) LL-37 docked to a DPC micelle. The coordinates of the micelle consisting of 65 DPC lipids and equilibrated with molecular dynamics in the presence of 6305 water molecules were downloaded from the Biocomputing Web Site at the University of Calgary (Department of Biological Sciences at the University of Calgary, http://moose.bio.ucalgary.ca/) and overlaid to the coordinates of the pseudomicelle sphere.

DISCUSSION

Previous structural studies by CD spectroscopy (*13, 14*) revealed that LL-37 assumes a random coil conformation in pure aqueous solution but a helical secondary structure in common structure-inducing environments like TFE or lipid bilayer vesicles. These studies correlated the helical content to the observed antibacterial activity of the peptide. Therefore, the accurate knowledge of the three-dimensional structure of the mature peptide is crucial to understand its function. Unfortunately, organic solvents cannot substitute for the bilayer structure of lipid membranes, and the data acquired so far on LL-37 in membranes did not allow for the determination of a high-resolution structure of the full-length peptide. On the other hand, DPC micelles are a reliable membrane mimetic model and have been utilized extensively for solution NMR studies of antimicrobial peptides (*27, 28, 39*−*47*) as well as integral membrane proteins (*30, 31, 44, 48*−*51*). In selected cases, DPC micelles preserve not only the native conformations of membrane proteins (*30*) but also membrane enzyme activity (*52, 53*). The activity of LL-37 has been measured by solid-state NMR experiments on model membranes containing LL-37 and lipids with phosphocholine headgroups (*14*). This not only justifies the choice of DPC but allows for further experiments characterizing membrane protein binding interfaces (*31, 52, 53*). Under our experimental conditions, LL-37 assumes a helix−break−helix conformation, with K12 located at the break point between the N-terminal and the C-terminal helices. The overall NOE pattern of LL-37 is reminiscent of that of pardaxin, another antimicrobial/toxin peptide that we studied in DPC micelles (*27*). As with pardaxin, most of the dipolar correlations are localized in the central region of LL-37, with several long-range NOEs present in the N-terminal region and very few NOEs in the C-terminal part of the peptide. In addition to the helix−break−helix motif, both peptides have the hydrophobic face of the amphipathic helix positioned toward the concave side. The central hinge region is a common motif in many antimicrobial peptides and is thought to provide for the conformational flexibility required for the formation of ion channels (*54, 55*). The N-terminal portions of both pardaxin and LL-37 are not ideal amphipathic helices and both terminate with a pair of phenylalanines (*27*). These residues are usually located at the water/lipid interface and may facilitate the insertion of the antimicrobial peptide in the lipid membranes. In pardaxin, the two phenylalanines make the N-terminal region structured, probably through $\pi-\pi$ interactions (*27*). On the contrary, the N-terminal domain of LL-37, which is necessary for the antimicrobial action, is not stabilized by the two phenylalanines and has a higher structural disorder, as demonstrated by the presence of sparse NOEs and H/D exchange experiments. In fact, if it is truncated, the peptide loses most of the antimicrobial potency against *Escherichia coli* bacteria. In spite of the structural and sequence similarities, the mechanisms of action for pardaxin and LL-37 are significantly different. While pardaxin is thought to operate through a "barrel-stave" model at a low peptide concentration and *via* a carpet model at higher concentrations (*27, 56*), recent solid-state NMR data suggest that LL-37 interaction with the membranes does not involve a "barrel-stave" mechanism; rather the carpet-toroidal-type mechanism of action was proposed (*14*). The structure and the topology of LL-37 that we obtained in detergent micelle support the latter mechanism with LL-37 in a helical conformation that is absorbed on the surface of the micelle.

Another important structural feature of LL-37 in DPC micelles is the pronounced curvature of the structure (see Figures 5 and 7), which we also observed in two variants of magainin peptides (MSI-78 and MSI-594) (*28*). The structural determinants for the curvatures in transmembrane and

amphipathic helices are unknown. However, a recent paper by Koeppe and co-workers (*60*) identified lysines as the possible cause of curvatures in membrane-associated peptides. All of these polypeptides (LL-37, MSI-78, and MSI-594) are lysine-rich, and the curvature may be due to the interactions that the lysine side chains make with the interfacial region of the micelle. Interestingly, a marked curvature of the two amphipathic helices was also observed for α-synuclein (*57, 58*), a membrane binding protein that has been associated with Parkinson's disease. α-Synuclein has six repeat regions that contain lysine residues (KTKEGV). A model of LL-37 interacting with the DPC micelle is depicted in Figure 8. It should be kept in mind that these studies in micelles represent only a starting point for our understanding of the interactions of LL-37 with membrane bilayers. In fact, a significant problem with detergent micelles is that the curvature of the micelle surface may induce structural deviations. To give a more realistic view of the interactions between LL-37 and lipid membranes, solution NMR data must be interpreted in the light of solid-state NMR results acquired in lipid bilayers. Assuming there are only slight deviations of the LL-37 structure in micelles from that in lipid bilayers (*59*) and including the PISEMA solid-state results obtained in mechanically oriented lipid bilayers (*15*), LL-37 appears to be adsorbed on the surface of the lipid membrane. Therefore, it is possible to hypothesize that LL-37 is mostly unstructured in solution and becomes helical upon interaction with lipid membranes. From the surface position, LL-37 can be depicted diffusing into the bacterial inner membrane and destroying it upon reaching MIC (*11, 14*). This is consistent with the *nonpore carpet-like* mechanism of action (*56*).

In conclusion, we have solved the three-dimensional structure of the mature LL-37 peptide embedded in DPC micelles. While the overall structure of LL-37 (helix−break−helix) is reminiscent of pardaxin, the different structural and dynamic details in the N-terminus might explain the different selectivity and mechanism of action of LL-37. Taken with the solid-state NMR results on phospholipid bilayers with varying composition (*11*), this study of LL-37 in micelles will help to pave the way for a detailed understanding of its interaction with lipid membranes and its role in human biochemical defense. Since knowledge of the structures of naturally occurring peptides such as LL-37 is essential to design more potent and selective antimicrobial peptides, the present study will be of significant value for designing efficient peptide fragments or de novo peptides for pharmaceutical applications. In addition, a comparison of the structural features and mechanism of LL-37 with other well-studied amphipathic α-helical antimicrobial peptides such as pardaxin (*27, 56*) and magainins (*28*) will lead to further insights for the development of new antimicrobial compounds of pharmaceutical importance to overcome the increasing bacterial resistance problem.

REFERENCES

1. Zasloff, M. (1987) Magainins, a Class of Antimicrobial Peptides from *Xenopus* Skin: Isolation, Characterization of Two Active Forms, and Partial cDNA Sequence of a Precursor. *Proc. Natl. Acad. Sci. U.S.A. 84*, 5449–5453.
2. Zasloff, M. (1992) Antibiotic Peptides as Mediators of Innate Immunity. *Curr. Opin. Immunol. 4*, 3–7.
3. Zanetti, M. (2005) The Role of Cathelicidins in the Innate Host Defenses of Mammals. *Curr. Issues Mol. Biol. 7*, 179–196.
4. Frohm, M., Agerberth, B., Ahangari, G., Stahle-Backdahl, M., Liden, S., Wigzell, H., and Gudmundsson, G. H. (1997) The Expression of the Gene Coding for the Antibacterial Peptide LL-37 is Induced in Human Keratinocytes during Inflammatory Disorders. *J. Biol. Chem. 272*, 15258–15263.
5. Tanaka, D., Miyasaki, K. T., and Lehrer, R. I. (2000) Sensitivity of *Actinobacillus Actinomycetemcomitans* and *Capnocytophaga* Spp. to the Bactericidal Action of LL-37: A Cathelicidin found in Human Leukocytes and Epithelium. *Oral Microbiol. Immunol. 15*, 226–231.
6. De, Y., Chen, Q., Schmidt, A. P., Anderson, G. M., Wang, J. M., Wooters, J., Oppenheim, J. J., and Chertov, O. (2000) LL-37, the Neutrophil Granule- and Epithelial Cell-Derived Cathelicidin, Utilizes Formyl Peptide Receptor-Like 1 (FPRL1) as a Receptor to Chemoattract Human Peripheral Blood Neutrophils, Monocytes, and T Cells. *J. Exp. Med. 192*, 1069–1074.
7. Tjabringa, G. S., Rabe, K. F., and Hiemstra, P. S. (2005) The Human Cathelicidin LL-37: A Multifunctional Peptide Involved in Infection and Inflammation in the Lung. *Pulm. Pharmacol. Ther. 18*, 321–327.
8. Bals, R., Weiner, D. J., Moscioni, A. D., Meegalla, R. L., and Wilson, J. M. (1999) Augmentation of Innate Host Defense by Expression of a Cathelicidin Antimicrobial Peptide. *Infect. Immun. 67*, 6084–6089.
9. Bals, R., Wang, X., Zasloff, M., and Wilson, J. M. (1998) The Peptide Antibiotic LL-37/hCAP-18 is Expressed in Epithelia of the Human Lung Where it has Broad Antimicrobial Activity at the Airway Surface. *Proc. Natl. Acad. Sci. U.S.A. 95*, 9541–9546.
10. Bergman, P., Walter-Jallow, L., Broliden, K., Agerberth, B., and Soderlund, J. (2007) The Antimicrobial Peptide LL-37 Inhibits HIV-1 Replication. *Curr. HIV Res. 5*, 410–415.
11. Durr, U. H., Sudheendra, U. S., and Ramamoorthy, A. (2006) LL-37, the Only Human Member of the Cathelicidin Family of Antimicrobial Peptides. *Biochim. Biophys. Acta 1758*, 1408–1425.
12. Li, X., Li, Y., Han, H., Miller, D. W., and Wang, G. (2006) Solution Structures of Human LL-37 Fragments and NMR-Based Identification of a Minimal Membrane-Targeting Antimicrobial and Anticancer Region. *J. Am. Chem. Soc. 128*, 5776–5785.
13. Johansson, J., Gudmundsson, G. H., Rottenberg, M. E., Berndt, K. D., and Agerberth, B. (1998) Conformation-Dependent Antibacterial Activity of the Naturally Occurring Human Peptide LL-37. *J. Biol. Chem. 273*, 3718–3724.
14. Henzler-Wildman, K. A., Lee, D. K., and Ramamoorthy, A. (2003) Mechanism of Lipid Bilayer Disruption by the Human Antimicrobial Peptide, LL-37. *Biochemistry 42*, 6545–6558.
15. Henzler-Wildman, K. A., Martinez, G. V., Brown, M. F., and Ramamoorthy, A. (2004) Perturbation of the Hydrophobic Core of Lipid Bilayers by the Human Antimicrobial Peptide LL-37. *Biochemistry 43*, 8459–8469.
16. Bax, A., and Davis, D. G. (1985) MLEV-17 Based Two-Dimensional Homonuclear Magnetization Transfer Spectroscopy. *J. Magn. Reson. 65*, 355–360.
17. Kumar, A., Ernst, R. R., and Wuthrich, K. (1980) A Two-Dimensional Nuclear Overhauser Enhancement (2D NOESY) Experiment for the Elucidation of Complete Proton-Proton Cross Relaxation Networks in Biological Macromolecules. *Biochem. Biophys. Res. Commun. 95*, 1–6.
18. Piotto, M., Saudek, V., and Skelnar, V. (1992) Gradient-Tailored Excitation for Single-Quantum NMR Spectroscopy of Aqueous Solution. *J. Biomol. NMR 2*, 661–665.
19. Shaka, A. J., Lee, C. J., and Pines, A. (1988) Iterative Schemes for Bilinear Operators: Application to Spin Decoupling. *J. Magn. Reson. 77*, 274–293.
20. Delaglio, F., Grzesiek, S., Vuister, G. W., Zhu, G., Pfeifer, J., and Bax, A. (1995) NMRPipe: A Multidimensional Spectral Processing System Based on UNIX Pipes. *J. Biomol. NMR 6*, 277–293.
21. Goddard, T., and Kneller D. G. (1999)SPARKY 3, San Francisco, CA.
22. Wuthrich, K. (1986) *NMR of Proteins and Nucleic Acids*, John Wiley & Sons, New York.
23. Schwieters, C. D., Kuszewski, J. J., Tjandra, N., and Clore, G. M. (2003) The XPLOR-NIH NMR Molecular Structure Determination Package. *J. Magn. Reson. 160*, 65–73.
24. Laskowski, R. A., Rullmannn, J. A., MacArthur, M. W., Kaptein, R., and Thornton, J. M. (1996) AQUA and PROCHECK-NMR: Programs for Checking the Quality of Protein Structures Solved by NMR. *J. Biomol. NMR 8*, 477–486.

25. Shi, L., Traaseth, N. J., Verardi, R., Gao, J., and Veglia, G. (2008) Paramagnetic-Based Pseudo-Micelle Potential to Determine Membrane Protein Topology in Detergent Micelles(submitted for publication).
26. Battiste, J. L., and Wagner, G. (2000) Utilization of Site-Directed Spin Labeling and High-Resolution Heteronuclear Nuclear Magnetic Resonance for Global Fold Determination of Large Proteins with Limited Nuclear Overhauser Effect Data. *Biochemistry 39*, 5355–5365.
27. Porcelli, F., Buck, B., Lee, D. K., Hallock, K. J., Ramamoorthy, A., and Veglia, G. (2004) Structure and Orientation of Pardaxin Determined by NMR Experiments in Model Membranes. *J. Biol. Chem. 279*, 45815–45823.
28. Porcelli, F., Buck-Koehntop, B. A., Thennarasu, S., Ramamoorthy, A., and Veglia, G. (2006) Structures of the Dimeric and Monomeric Variants of Magainin Antimicrobial Peptides (MSI-78 and MSI-594) in Micelles and Bilayers, Determined by NMR Spectroscopy. *Biochemistry 45*, 5793–5799.
29. Veglia, G., Zeri, A. C., Ma, C., and Opella, S. J. (2002) Deuterium/Hydrogen Exchange Factors Measured by Solution Nuclear Magnetic Resonance Spectroscopy as Indicators of the Structure and Topology of Membrane Proteins. *Biophys. J. 82*, 2176–2183.
30. Zamoon, J., Mascioni, A., Thomas, D. D., and Veglia, G. (2003) NMR Solution Structure and Topological Orientation of Monomeric Phospholamban in Dodecylphosphocholine Micelles. *Biophys. J. 85*, 2589–2598.
31. Buffy, J. J., Buck, B. A., Porcelli, F., Traaseth, N. J., Thomas, D. D., and Veglia, G. (2006) Defining the Intramembrane Binding Mechanism of Sarcolipin to Calcium ATPase using Solution NMR Spectroscopy. *J. Mol. Biol. 358*, 420–429.
32. Cheng, R. P., Girinath, P., and Ahmad, R. (2007) Effect of Lysine Side Chain Length on Intra-Helical Glutamate-Lysine Ion Pairing Interactions. *Biochemistry 46*, 10528–10537.
33. Egal, M., Conrad, M., MacDonald, D. L., Maloy, W. L., Motley, M., and Genco, C. A. (1999) Antiviral Effects of Synthetic Membrane-Active Peptides on Herpes Simplex Virus, Type 1. *Int. J. Antimicrob. Agents 13*, 57–60.
34. Egal, M., Conrad, M., MacDonald, D. L., Maloy, W. L., Motley, M., and Genco, C. A. (1999) Antiviral Effects of Synthetic Membrane-Active Peptides on Herpes Simplex Virus, Type 1. *Int. J. Antimicrob. Agents 13*, 57–60.
35. Charpentier, S., Amiche, M., Mester, J., Vouille, V., Le Caer, J. P., Nicolas, P., and Delfour, A. (1998) Structure, Synthesis, and Molecular Cloning of Dermaseptins B, a Family of Skin Peptide Antibiotics. *J. Biol. Chem. 273*, 14690–14697.
36. Wechselberger, C. (1998) Cloning of cDNAs Encoding New Peptides of the Dermaseptin-Family. *Biochim. Biophys. Acta 1388*, 279–283.
37. Mor, A., Hani, K., and Nicolas, P. (1994) The Vertebrate Peptide Antibiotics Dermaseptins have Overlapping Structural Features but Target Specific Microorganisms. *J. Biol. Chem. 269*, 31635–31641.
38. Rao, A. G., Hassan, M., and Hempel, J. C. (1994) Structure-Function Validation of High Lysine Analogs of Alpha-Hordothionin Designed by Protein Modeling. *Protein Eng. 7*, 1485–1493.
39. Campagna, S., Saint, N., Molle, G., and Aumelas, A. (2007) Structure and Mechanism of Action of the Antimicrobial Peptide Piscidin. *Biochemistry 46*, 1771–1778.
40. Ovchinnikova, T. V., Shenkarev, Z. O., Nadezhdin, K. D., Balandin, S. V., Zhmak, M. N., Kudelina, I. A., Finkina, E. I., Kokryakov, V. N., and Arseniev, A. S. (2007) Recombinant Expression, Synthesis, Purification, and Solution Structure of Arenicin. *Biochem. Biophys. Res. Commun. 360*, 156–162.
41. Powers, J. P., Tan, A., Ramamoorthy, A., and Hancock, R. E. (2005) Solution Structure and Interaction of the Antimicrobial Polyphemusins with Lipid Membranes. *Biochemistry 44*, 15504–15513.
42. Hicks, R. P., Mones, E., Kim, H., Koser, B. W., Nichols, D. A., and Bhattacharjee, A. K. (2003) Comparison of the Conformation and Electrostatic Surface Properties of Magainin Peptides Bound to Sodium Dodecyl Sulfate and Dodecylphosphocholine Micelles. *Biopolymers 68*, 459–470.
43. Javadpour, M. M., and Barkley, M. D. (1997) Self-Assembly of Designed Antimicrobial Peptides in Solution and Micelles. *Biochemistry 36*, 9540–9549.
44. Gesell, J., Zasloff, M., and Opella, S. J. (1997) Two-Dimensional ^{1}H NMR Experiments show that the 23-Residue Magainin Antibiotic Peptide is an Alpha-Helix in Dodecylphosphocholine Micelles, Sodium Dodecylsulfate Micelles, and trifluoroethanol/water Solution. *J. Biomol. NMR 9*, 127–135.
45. Park, K., Oh, D., Shin, S. Y., Hahm, K. S., and Kim, Y. (2002) Structural Studies of Porcine Myeloid Antibacterial Peptide PMAP-23 and its Analogues in DPC Micelles by NMR Spectroscopy. *Biochem. Biophys. Res. Commun. 290*, 204–212.
46. Rozek, A., Friedrich, C. L., and Hancock, R. E. (2000) Structure of the Bovine Antimicrobial Peptide Indolicidin Bound to Dodecylphosphocholine and Sodium Dodecyl Sulfate Micelles. *Biochemistry 39*, 15765–15774.
47. Roumestand, C., Louis, V., Aumelas, A., Grassy, G., Calas, B., and Chavanieu, A. (1998) Oligomerization of Protegrin-1 in the Presence of DPC Micelles. A Proton High-Resolution NMR Study. *FEBS Lett. 421*, 263–267.
48. Jaroniec, C. P., Kaufman, J. D., Stahl, S. J., Viard, M., Blumenthal, R., Wingfield, P. T., and Bax, A. (2005) Structure and Dynamics of Micelle-Associated Human Immunodeficiency Virus gp41 Fusion Domain. *Biochemistry 44*, 16167–16180.
49. Arora, A., Abildgaard, F., Bushweller, J. H., and Tamm, L. K. (2001) Structure of Outer Membrane Protein A Transmembrane Domain by NMR Spectroscopy. *Nat. Struct. Biol. 8*, 334–338.
50. MacKenzie, K. R., Prestegard, J. H., and Engelman, D. M. (1997) A Transmembrane Helix Dimer: Structure and Implications. *Science 276*, 131–133.
51. Traaseth, N. J., Verardi, R., Torgersen, K. D., Karim, C. B., Thomas, D. D., and Veglia, G. (2007) Spectroscopic Validation of the Pentameric Structure of Phospholamban. *Proc. Natl. Acad. Sci. U.S.A. 104*, 14676–14681.
52. Zamoon, J., Nitu, F., Karim, C., Thomas, D. D., and Veglia, G. (2005) Mapping the Interaction Surface of a Membrane Protein: Unveiling the Conformational Switch of Phospholamban in Calcium Pump Regulation. *Proc. Natl. Acad. Sci. U.S.A. 102*, 4747–4752.
53. Traaseth, N. J., Thomas, D. D., and Veglia, G. (2006) Effects of Ser16 Phosphorylation on the Allosteric Transitions of Phospholamban/Ca^{2+}-ATPase Complex. *J. Mol. Biol. 358*, 1041–1050.
54. Oh, D., Shin, S. Y., Kang, J. H., Hahm, K. S., Kim, K. L., and Kim, Y. (1999) NMR Structural Characterization of Cecropin A(1−8)−Magainin 2(1−12) and Cecropin A (1−8)−Melittin (1−12) Hybrid Peptides. *J. Pept. Res. 53*, 578–589.
55. Oh, D., Shin, S. Y., Lee, S., Kang, J. H., Kim, S. D., Ryu, P. D., Hahm, K. S., and Kim, Y. (2000) Role of the Hinge Region and the Tryptophan Residue in the Synthetic Antimicrobial Peptides, Cecropin A(1−8)−Magainin 2(1−12) and its Analogues, on their Antibiotic Activities and Structures. *Biochemistry 39*, 11855–11864.
56. Hallock, K. J., Lee, D., Omnaas, J., Mosberg, H. I., and Ramamoorthy, A. (2002) Membrane Composition Determines Pardaxin's Mechanism of Lipid Bilayer Disruption. *Biophys. J. 83*, 1004–1013.
57. Ulmer, T. S., and Bax, A. (2005) Comparison of Structure and Dynamics of Micelle-Bound Human Alpha-Synuclein and Parkinson Disease Variants. *J. Biol. Chem. 280*, 43179–43187.
58. Ulmer, T. S., Bax, A., Cole, N. B., and Nussbaum, R. L. (2005) Structure and Dynamics of Micelle-Bound Human Alpha-Synuclein. *J. Biol. Chem. 280*, 9595–9603.
59. Franzin, C. M., Teriete, P., and Marassi, F. M. (2007) Structural Similarity of a Membrane Protein in Micelles and Membranes. *J. Am. Chem. Soc. 129*, 8078–8079.
60. Daily, A. E., Greathouse, D. V., van der Wel, P. C. A., and Koeppe, R. E. (2008) Helical Distortion in Tryptophan and Lysine Anchored Membrane-Spanning Alpha Helices as a Function of Hydrophobic Mismatch: A Solid-State Deuterium NMR Investigation using the GALA Method. *Biophys. J. 94*, 480–491.

BI702036S